NEGF-HF Method in Molecular Junction Property Calculations

MICHAEL GALPERIN[a] AND ABRAHAM NITZAN[b]

[a]*P.M. Gross Chemical Laboratory, Duke University, Durham, North Carolina, USA*

[b]*School of Chemistry, Tel Aviv University, Tel Aviv, Israel*

ABSTRACT: Electron–electron interaction is an essential issue in predicting the properties of a molecular conduction junction. An accurate treatment requires taking proper account of the potential distribution across the junction as well as for the change in electronic structure under the external voltage drop. Another important point is the necessity to treat molecules as open quantum systems. In this paper we address these issues within the framework of the non-equilibrium Green's function formalism at the Hartree–Fock level (NEGF-HF), which permits a self-consistent treatment of the problem. We apply the method to study the experimentally observed asymmetry in the *I–V* curves with respect to polarity of voltage bias in Hg–Au junctions containing bilayers of alkanethiols of various chain lengths. The origin of the effect is suggested to be the asymmetric behavior of the character of the highest occupied molecular orbital (HOMO) of the junction at opposite biases, which leads to different effective barriers for electron transfer across the junction at opposite signs of the voltage drop. The calculated potential profile shows the capacitor-like nature for the junction with the weak link.

KEYWORDS: molecular electronics; rectification; nonequilibrium Green's function; molecular capacitors

INTRODUCTION

The study of molecular conduction junctions brings into focus some outstanding theoretical issues related to the fact that we are dealing with open non-equilibrium quantum systems carrying fluxes of both charge carriers and energy. Taking into account the open character of the junction amounts to considering electronic structure and dynamic response in a non-equilibrium *grand canonical* situation. Thus, scattering theory based considerations that lead, for example, to the Landauer expression[1,2] for the conduction, may not be adequate. Instead, the non-equilibrium Green's function technique, invented independently by Keldysh[3] and Kadanoff and Baym[4] provides a powerful tool for addressing such problems. Here we apply this technique to study molecular junctions under bias with electron–electron interaction taken into account at the HF level of theory and use it to address conduction in bimolecular alkane junctions. Although there are no principle obstacles in taking into

Address for correspondence: Abraham Nitzan, School of Chemistry, Tel Aviv University, Tel Aviv 69978, Israel. Voice: 972-3-640 8904; fax: 972-3-642 3765.
nitzan@post.tau.ac.il

Ann. N.Y. Acad. Sci. **1006: 48–67 (2003).**
doi: 10.1196/annals.1292.003

account correlation effects as well, the HF level of theory allows a self-consistent procedure implied by the technique to be implemented in a very efficient form.

An important attribute of a biased molecular junction is the potential distribution along it. A demonstration of the importance of this issue to the understanding of the current–voltage behavior was recently presented by Datta and coworkers[5,6] who have shown, within a simple extended Huckel (EH) model for α,α'-xylyl dithiol bridging between two gold leads, that the potential profile (imposed as input to the EH calculation) exerted a profound effect on quantitative as well as qualitative aspects of the calculated current–voltage characteristic. Subsequent studies[7–12] calculate the potential distribution self consistently with the electronic structure calculation. In this work we follow an approach similar to that used by Damle and coworkers,[10] in which the electronic density in the non-equilibrium steady state molecular wire is computed using the NEGF methodology, followed by the Hartree potential evaluation—all under the imposed potential bias.

Non linearity of the current–voltage characteristic of a given junction, and the symmetry (or its absence) of the current under bias inversion are (related) important properties of the junction. Asymmetry, that is, rectification property, was observed in several systems involving monolayer and multilayer films as well as single molecule junctions.[13–20] Several theoretical discussions of this issue have been published,[21–24] starting with the original prediction of molecular rectification by Aviram and Ratner.[21]

Recent experimental results by Sek and Majda[25] show asymmetry in the current–voltage characteristic of the Hg–Au junctions incorporating a bilayer of alkanethiol films of varying chain length. Current rectification was observed for all asymmetric junctions, such that a larger current was seen when the longer alkanethiol segment is attached to the negatively biased electrode. In this paper we provide a detailed account of our theoretical interpretation of this experiment,[25] using a simple model system that is treated within the NEGF-HF theory. The simplicity of this model makes it possible to explain the physical source of the observed *I–V* asymmetry that more rigorous approaches tend to obscure.

In the next section we briefly review the NEGF-HF method for our problem. Subsequently, we present the molecular model used to simulate the experimental results on the *I–V* characteristic of biased bialkane junctions and then present and discuss the results of our estimates.

METHOD

We consider an open quantum system consisting of a single molecule (bridge) coupled to metallic leads *L* (left) and *R* (right), modeled as free electrons reservoirs, each in its own equilibrium. The electrons on the bridge interact with each other and with the externally imposed potential. The latter is taken as linear voltage drop, $\Delta V = V_L - V_R$, between the leads that are held at different electrochemical potentials $\mu_L = E_F - eV_L$ and $\mu_R = E_F - eV_R$ (e denotes the absolute value of electron charge). The Hamiltonian is a sum of terms associated with the molecule, the leads, the molecule–lead interactions and the external potential

$$H = H_M + H_{\text{Leads}} + H_{M-\text{Leads}} + H_{\text{external}}. \quad \textbf{(1)}$$

We represent this Hamiltonian in terms of an orthonormal basis set of single electron states. This can be in principle any orthonormal basis. Below we use the set $\{\psi\}$ obtained from a Löwdin transformation[26] of the atomic orbitals (AO) basis $\{\phi\}$. This transformation is defined by

$$\begin{cases} \psi_i^*(\vec{r}) = \sum_\alpha \phi_\alpha^*(\vec{r})[S^{-1/2}]_{i\alpha} \\ \psi_i(\vec{r}) = \sum_\alpha \phi_\alpha(\vec{r})[S^{-1/2}]_{\alpha i} \end{cases} \quad \textbf{(2)}$$

where S is the AO overlap matrix. Here and below we use Greek indices for atomic orbitals. Latin indices denote Löwdin orbitals.

The various terms in the Hamiltonian **(1)** may be written in the ††† second quantization representation in the forms

$$H_M = \sum_{i,\,j;\sigma} H_{ij}^c \hat{c}_{i;\sigma}^\dagger \hat{c}_{j;\sigma} + \frac{1}{2} \sum_{i_1,\,i_2,\,i_3,\,i_4} \sum_{\sigma_1,\,\sigma_2} V_{i_3 i_4}^{i_1 i_2} \hat{c}_{i_1,\,\sigma_1}^\dagger \hat{c}_{i_2,\,\sigma_2}^\dagger \hat{c}_{i_4,\,\sigma_2} \hat{c}_{i_3,\,\sigma_1}, \quad \textbf{(3)}$$

$$H_{\text{leads}} = \sum_{k \in L,\,R} \sum_\sigma \varepsilon_k \hat{c}_{k;\sigma}^\dagger \hat{c}_{k;\sigma}, \quad \textbf{(4)}$$

$$H_{M-\text{leads}} = \sum_{k \in L,\,R} \sum_\sigma \sum_i (V_{ki} \hat{c}_{k;\sigma}^\dagger \hat{c}_{i;\sigma} + \text{h.c.}), \text{ and} \quad \textbf{(5)}$$

$$H_{\text{ext}} = \sum_{i,\,j;\sigma} V_{ij}^{\text{ext}} \hat{c}_{i;\sigma}^\dagger \hat{c}_{j;\sigma}, \quad \textbf{(6)}$$

where i, j are labels of the various Löwdin orbitals, $\hat{c}$ and $\hat{c}^\dagger$ are annihilation and creation operators in the corresponding Löwdin orbitals, $\sigma = \uparrow,\downarrow$ is the spin index, and k denotes (free) electron states in the contacts L and R.

The molecular Hamiltonian, Eq. **(3)**, contains a single electron part (the core Hamiltonian H^c) that arises from the (constant) core energy, the electron kinetic energy, and the core–electron interaction; and a two electron part that accounts for the electron–electron interaction. In the latter, the tensor $V_{i_3 i_4}^{i_1 i_2}$ is the Löwdin transform of the AO two-center integrals

$$V_{\alpha_3 \alpha_4}^{\alpha_1 \alpha_2} = \int d\mathbf{r}_1 \int d\mathbf{r}_2 \varphi_{\alpha_1}^*(\mathbf{r}_1) \varphi_{\alpha_2}^*(\mathbf{r}_2) \frac{e^2}{|\mathbf{r}_1 - \mathbf{r}_2|} \varphi_{\alpha_3}(\mathbf{r}_1) \varphi_{\alpha_4}(\mathbf{r}_2). \quad \textbf{(7)}$$

The leads, Eq. **(4)**, are represented by a free electron Hamiltonian. The molecule–lead interaction, Eq. **(5)**, is taken to be of a single electron type that creates (destroys) an electron on the molecule while destroying (creating) it in one of the leads. Finally, H_{ext}, given by Eq. **(6)**, represents the external bias.

Consider the latter contribution to H. For a given external electrostatic potential

$$\Phi_{\text{ext}}(\mathbf{r}) = -\mathbf{E}_{\text{ext}} \cdot \mathbf{r}, \quad \textbf{(8)}$$

the interaction is

$$H_{\text{ext}} = \int d\mathbf{r} \hat{\rho}_{\text{el}}(\mathbf{r}) \Phi_{\text{ext}}(\mathbf{r}), \quad \textbf{(9)}$$

where $\hat{\rho}_{\text{el}}(\mathbf{r})$ is the electronic charge density operator

$$\hat{\rho}_{\text{el}}(\mathbf{r}) = -e\hat{n}(\mathbf{r}) = -e\hat{\psi}^\dagger(\mathbf{r})\hat{\psi}(\mathbf{r}). \quad \textbf{(10)}$$

$$\hat{\psi}(\mathbf{r}) \equiv \sum_j \hat{c}_j \psi_j(\mathbf{r}), \quad \textbf{(11)}$$

where $\psi_j(\mathbf{r})$ are the Lowdin orbitals. Note that the constant contribution of the nuclear charge density to H_{ext} has been disregarded. Using **(2)**, **(8)**, **(10)**, and **(11)** in **(9)** one obtains

$$V_{ij}^{\text{ext}} = -\mathbf{E} \cdot \mathbf{M}_{ij}, \tag{12}$$

where $\mathbf{M}_{ij}$ is the electronic dipole moment integral in the orthonormal basis, which is the Löwdin transformation of the corresponding quantity in the atomic orbital basis

$$\mathbf{M}_{ij} = -e \sum_{\alpha,\beta} [S^{-1/2}]_{i\alpha} \int d\mathbf{r} \phi_\alpha^*(\mathbf{r}) \mathbf{r} \phi_\beta(\mathbf{r}) [S^{-1/2}]_{\beta j}. \tag{13}$$

Next we use the NEGF technique[3,4] to calculate the electronic transport properties of this system. In this calculation the single-electron part of the molecular Hamiltonian **(3)** and the leads Hamiltonian **(4)** constitute the zero-order Hamiltonian, whereas the molecule–lead coupling, the interaction with the external potential (an alternative could be to combine H_{ext} of Eq. **(6)** with the single electron part of Eq. **(3)**), and the electron–electron interaction on the molecule are taken as perturbations. Because we are interested in the steady-state current, we can restrict consideration to the Keldysh contour and allow energy domain calculation of the Green functions and self-energies. The total self-energy of the molecular bridge is approximated by a sum of independent terms associated with the various perturbations

$$\Sigma = \Sigma^L + \Sigma^R + \Sigma^{\text{ext}} + \Sigma^{e-e}. \tag{14}$$

We use standard perturbation expansion with truncation at the lowest nonzero order in interactions. In this order Σ^L, Σ^R, and Σ^{ext} are obtained exactly, whereas Σ^{e-e} is obtained on the Hartree–Fock level. On the Keldysh contour the self-energies due to coupling to the leads are

$$\Sigma_{ij;\sigma}^K(\tau_1, \tau_2) = \sum_{k \in K} V_{ki}^* G_{k;\sigma}^K(\tau_1, \tau_2) V_{kj}, \quad K = L, R, \tag{15}$$

where $G_{k;\sigma}^K(\tau_1, \tau_2)$ is the contour ordered (Keldysh contour) free electron Green function of the electrode K and τ is the contour variable. The self-energy associated with the external potential takes the form

$$\Sigma_{ij;\sigma}^{\text{ext}}(\tau_1, \tau_2) = \delta(\tau_1, \tau_2) V_{ij}^{\text{ext}} \tag{16}$$

and the HF self energy is

$$\begin{aligned} (\Sigma^{e-e})_{ij,\sigma} &= (\Sigma_{HF})_{ij,\sigma} \\ &= i\delta(\tau_1, \tau_2) \sum_{l,m} \{ V_{jm}^{il} [G_{ml;\sigma}(\tau_1, \tau_1^+) + G_{ml;\bar{\sigma}}(\tau_1, \tau_1^+)] - V_{jm}^{il} G_{ml;\sigma}(\tau_1, \tau_1^+) \}. \end{aligned} \tag{17}$$

Here $G_{ml;\sigma}(\tau_1, \tau_1^+)$ is the molecular Green's function on the Keldysh contour, and σ and $\bar{\sigma}$ denote opposite spin projections. Note that $\hbar = 1$ is used throughout.

Projecting the contour related quantities to the real time axis gives rise to retarded and advanced, $\Sigma^r = [\Sigma^a]^\dagger$, lesser, $\Sigma^<$, and greater, $\Sigma^>$, self-energies. For semi-infinite free electron metals or for metals represented by a tight-binding model with non-interacting electrons, the self-energies **(15)** due to the contacts may be evaluated exactly. Particularly simple results are obtained in the wide band limit for the lead, where the real part of the retarded (advanced) self-energies is disregarded and the Fourier transform of their imaginary part is taken to be energy independent. Furthermore, since we take the contacts to be in equilibrium, the lesser and greater

self-energies are obtained from the fluctuation-dissipation theorem. Then, in energy space,

$$\begin{aligned} [\Sigma_K^r]_{ij;\sigma} &= -i\frac{\gamma_{ij}^K}{2} \\ [\Sigma_K^<]_{ij;\sigma} &= i\gamma_{ij}^K f_K(E) \qquad\qquad K = R, L, \\ [\Sigma_K^>]_{ij;\sigma} &= -i\gamma_{ij}^K[1 - f_K(E)] \end{aligned} \tag{18}$$

where $f_K(E)$ is a Fermi–Dirac distribution characterized by the corresponding chemical potential μ_K.

The (contour) time-local self-energies arising from the external potential and the electron–electron interaction on the bridge give rise to the retarded (advanced) projections only. The corresponding lesser and greater projections of such time-local quantities vanish by definition. Also, the time locality implies that the Fourier transform of the advanced (retarded) GFs are energy independent. Explicitly, in energy space,

$$(\Sigma_{\text{ext}}^r)_{ij} = V_{ij}^{\text{ext}} \tag{19}$$

for either spin direction and

$$[\Sigma_{HF}^r]_{ij;\uparrow} = \sum_{l,m}(V_{jm}^{il}[P_{ml;\uparrow} + P_{ml;\downarrow}] - V_{mj}^{il}P_{ml;\uparrow}), \tag{20}$$

with an equivalent equation for the opposite spin. In **(20)** the first term is the Coulomb interaction, the second term is the exchange integral, and $P_{mk;\sigma}$ are elements of the density matrix. The latter are obtained from the molecule lesser GF

$$P_{ml;\sigma} = -i\int_{-\infty}^{\infty}\frac{dE}{2\pi}G_{ml;\sigma}^<(E). \tag{21}$$

The calculation is performed in a standard way, solving simultaneously the Dyson equation for the retarded (advanced) Green's function and the Keldysh equation for the lesser (greater) projection. (It is sufficient to focus on the two projections, say, retarded and lesser, since for consideration restricted to the Keldysh contour there are only two independent quantities: $G^a = [G^r]^+$ and $G^r - G^a = G^> - G^<$.)

$$G^{r,a}(E) = [E - H^c - \Sigma^{r,a}]^{-1} \tag{22}$$

$$G^{<,>}(E) = G^r(E)\Sigma^{<,>}(E)G^a(E). \tag{23}$$

Here, H^c stands for the single-electron core Hamiltonian (first term of Eq. **(3)**) and $\Sigma^{r,a}$ are sums of all contributions to the retarded (advanced) self-energy according to **(14)**. These two equations are coupled: to calculate, say, the retarded Green function of Eq. **(22)** we need the self energies from Eqs. **(18)**–**(20)**, whereas the HF self-energy, Eq. **(20)**, is calculated from the density matrix, Eq. **(21)**, which in turn depends on the lesser Green function, Eq. **(23)**.

Since our problem is spin-symmetric, it is sufficient in a restricted HF calculation to consider only one spin coordinate, so the spin index is henceforth omitted. Equations **(22)** and **(23)** are solved iteratively, using Eqs. **(18)**–**(21)** by the following sequence of steps (see also FIGURE 1 for the algorithmic scheme):

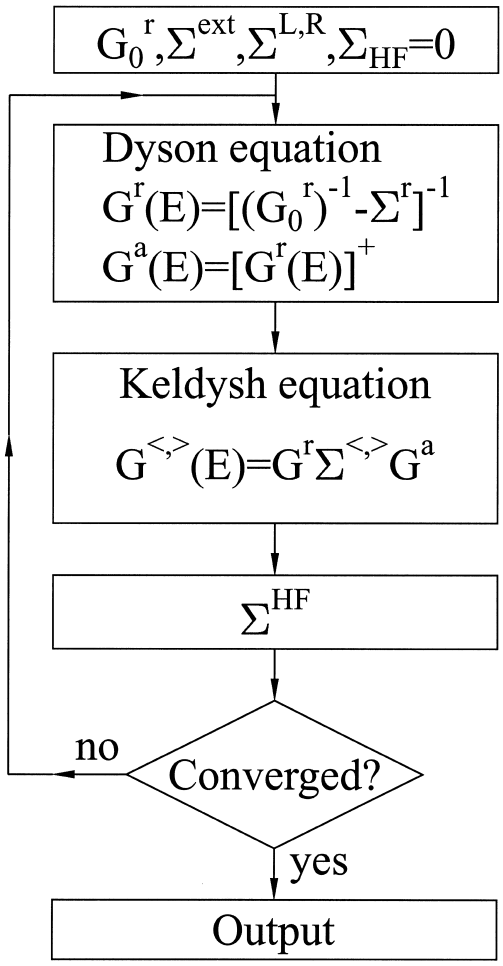

FIGURE 1. Algorithmic scheme of the self-consistent iterative procedure.

1. For the given values of the electrochemical potentials of the electrodes, μ_K ($K = L,R$), calculate the self-energies due to the leads from **(18)**. Calculate the external potential matrix, that is, the self-energy of **(19)**. The HF self-energy, **(20)**, is set to zero at the first step of iteration.
2. Compute the retarded (advanced) and the lesser (greater) self-energies of the molecular bridge using Eq. **(14)**.
3. Calculate the retarded (advanced) and lesser (greater) Green's functions from Eqs. **(22)** and **(23)**.
4. Calculate the density matrix from **(21)** and use it to update the HF self-energy according to **(20)**.

5. Check for convergence. Convergence is achieved when

$$\left|\frac{[\Sigma_{HF}]_{ij}^{(l+1)} - [\Sigma_{HF}]_{ij}^{(l)}}{[\Sigma_{HF}]_{ij}^{(l)}}\right| < \delta \quad \forall i, j,$$

where l is the iteration step and δ is a predefined tolerance. If convergence has not yet been achieved return to step 2.

Generally, the problem should be presented on an energy grid large enough to span the energy range relevant for the process under study, and dense enough for accurate evaluation of the integral in Eq. **(21)**. For large systems this leads to huge demand on memory and CPU time needed for the evaluation of the G and Σ matrices (in particular the need to invert, at each iteration, big matrices at each point of the energy grid). At the HF level of theory and when Eqs. **(18)** hold for the self-energy elements associated with the molecule–metal coupling, one can simplify the procedure (see APPENDIX) so that there is no need for a brute force numerical evaluation of the integral in Eq. **(21)**.

After the procedure has converged, the current through the junction is obtained from the Landauer formula,[1,2]

$$I = -\frac{2e}{\hbar}\int_{-\infty}^{\infty}\frac{dE}{2\pi}Tr[\Gamma_L(E)G^r(E)\Gamma_R(E)G^a(E)](f_L(E) - f_R(E)), \qquad \textbf{(24)}$$

where a factor of 2 accounts for the electron spin states, the trace is taken over the subspace of the molecular bridge, and

$$\Gamma_K(E) = i[\Sigma_K^r(E) - \Sigma_K^a(E)], \quad K = L, R. \qquad \textbf{(25)}$$

Note that Eq. **(24)** is applicable only for coherent transport. (In the literature on bridge assisted tunneling, "coherent electron tunneling" is the term used to describe electron tunneling undisturbed by phase destroying thermal motions of the nuclei.) The present consideration is restricted to the HF level of the theory in which electron-electron interaction does not destroy coherence. In the general case (e.g., when higher order terms in perturbation expansion are taken into account or if electron–phonon interaction is present) a more general expression for the current should be used (see e.g., Ref. 27).

Next consider the electrostatic potential on the molecule. This is the sum of the external potential **(8)** and the molecular potential due to the charge distribution on the bridge. We assume for simplicity that all the external potential falls on the space between the metal leads that encompass the molecular bridge. In reality part the imposed potential falls on the leads themselves.

$$\Phi_{\text{mol}}(\mathbf{r}) = \int d\mathbf{r}'\frac{\rho(\mathbf{r}')}{|\mathbf{r} - \mathbf{r}'|} = \Phi_{\text{nuc}}(\mathbf{r}) + \Phi_{\text{el}}(\mathbf{r}), \qquad \textbf{(26)}$$

where $\rho(\mathbf{r}) = \rho_{\text{nuc}}(\mathbf{r}) + \rho_{\text{el}}(\mathbf{r})$ is the charge distribution on the molecule, $\rho_{\text{nuc}}(\mathbf{r}) = \Sigma_n Z_n \delta(\mathbf{r} - \mathbf{R}_n)$ is fixed and, therefore, so is $\phi_{\text{nuc}}(\mathbf{r})$, and $\rho_{\text{el}}(\mathbf{r})$ is obtained from the self consistent calculation. Using **(10)**, **(11)**, and **(2)** one obtains for the electronic contribution

$$\Phi_{\text{el}}(\mathbf{r}) = -2e\sum_{i,j}P_{ji}\sum_{\alpha,\beta}[S^{-1/2}]_{i\alpha}\int d\mathbf{r}'\frac{\phi_\alpha^*(\mathbf{r}')\phi_\beta(\mathbf{r}')}{|\mathbf{r} - \mathbf{r}'|}[S^{-1/2}]_{\beta j}, \qquad \textbf{(27)}$$

where the factor 2 comes from the spin and P_{ij} is given by **(21)**. Equation **(27)** is our working expression for the electrostatic charge distribution.

APPLICATION TO BIMOLECULAR ALKANE–THIOL JUNCTIONS

In this section we apply the calculation procedure we have described to the experimental studies of Sek and Majda on the current–voltage characteristic in symmetric and asymmetric alkane–thiol bilayer junctions.[25] A previous report of the theoretical results is also provided in Reference 25. We consider a simple model (see FIGURE 2) consisting of two planar metal electrodes connected by a single pair of alkane–thiol molecules, each attached by its thiol end to its corresponding electrode. (This is a simplification, and in general other orientations need to be considered, e.g., alkanethiol adsorb on gold with a tilt angle of 30°.) We represent this junction schematically by L–S–$(CH_2)_n$–CH_3…CH_3–$(CH_2)_m$–S–R, where, as before, *L* and *R* denote the left and the right electrodes and … denotes the van-der-Waals gap between the molecular species. In the calculations presented below we consider

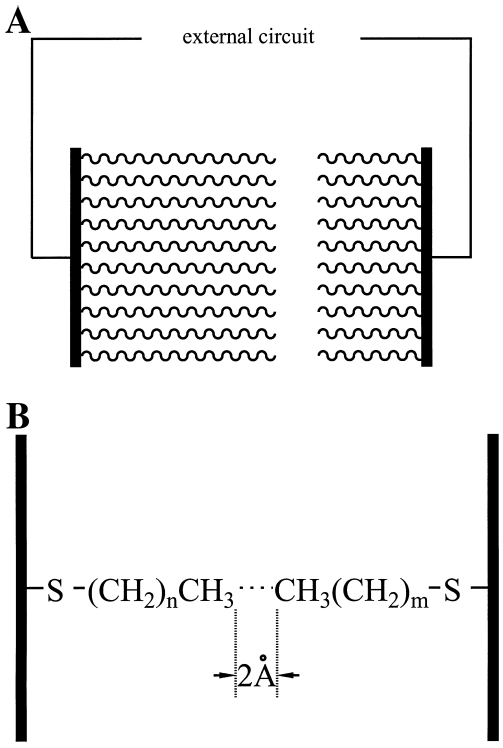

FIGURE 2. A. Schematic view of a Hg–Au alkanethiol bilayer junction. **B.** A single molecule model used in the calculations.

junctions with $n + m = 6$, both symmetric ($n = m = 3$) and asymmetric (e.g., $n = 5$, $m = 1$). Because we are interested in the general phenomenology rather than in details of any particular model we set up the junction geometry by artificially shifting apart the two segments of an $(n + m)$ alkane molecule to a distance 2 Å between the corresponding carbon centers. Also for simplicity, the two electrodes are treated as identical semi-infinite reservoirs of free electrons at thermal equilibrium. However, in the asymmetric junctions we use configurations in which the longer molecular chain is attached to the L (left) electrode, thus associating it with the Hg electrode in the experiment.[25]

For the molecular atomic orbitals we used the LANL2DZ basis set. With the (contracted) gaussian form of basis functions, the molecular dipole moment integrals **(13)** can be easily calculated by the corresponding contraction of overlap integrals between primitive gaussians, whereas the electronic part of electrostatic potential **(27)** is calculated by contraction of the nuclear attraction integrals.[28,29] The core Hamiltonian and the two-center integrals are computed using the GAUSSIAN package.[30] To conform with the bounds imposed by the use of the restricted HF (RHF) we performed our calculations on the closed-shell molecular structures L–HS–$(CH_2)_n$–CH_3…CH_3–$(CH_2)_m$–SH–R and assigned the self-energies due to the contacts, Eq. **(18)**, to the terminal S atoms, so that

$$\gamma^K_{\alpha\beta} = \gamma\delta_{\alpha\beta}\big|_{\alpha \in S_K}, \quad K = L, R, \tag{28}$$

where S_K denotes left ($K = L$) or right ($K = R$) sulphur atoms and where α and β are AOs. The value of γ, Eq. **(18)**, was arbitrarily chosen to be 0.2 eV (an order of magnitude estimate of the inverse lifetime for the decay of an excess electron on the S atom into the continuum of metal electronic states if the latter are unoccupied) for both electrodes.

The calculated current–voltage characteristic depends on the alignment of the molecular levels relative to the metal Fermi energies. In the calculations described below we chose the Fermi levels of the unbiased electrodes to be in the middle of the HOMO–LUMO gap of free unseparated alkyl-dithiol (HS–$(CH_2)_n$–SH) molecules as computed by the GAUSSIAN package.[30] Specifically, $E_F = -0.15$ a.u. was chosen for our HF calculations. The HOMO–LUMO gaps of the separated structures HS–$(CH_2)_n$–CH_3…CH_3–$(CH_2)_m$–SH are only slightly different. We found that different choices of Fermi energies did not influence the qualitative picture presented below.

FIGURE 3A shows the current–voltage characteristics for the symmetric and asymmetric junctions obtained by this NEGF-HF calculation. The I–V characteristic of the symmetric junction is symmetric under voltage polarity change, whereas the non-symmetric junction behaves asymmetrically, so that the current increases more rapidly when the left electrode (on which the longer molecular chain is attached) is biased negatively. FIGURE 3B shows that observed asymmetry in the I–V behavior increases with increasing asymmetry in the molecular structure. This behavior is in agreement with the experimental results. It should be emphasized that the agreement is qualitative only. In particular, the gap between thresholds of current setup is much larger than observed. Indeed the HF approximation is known to overestimate the HOMO–LUMO gap (see, e.g., Ref. 31). Another source of overestimating this gap

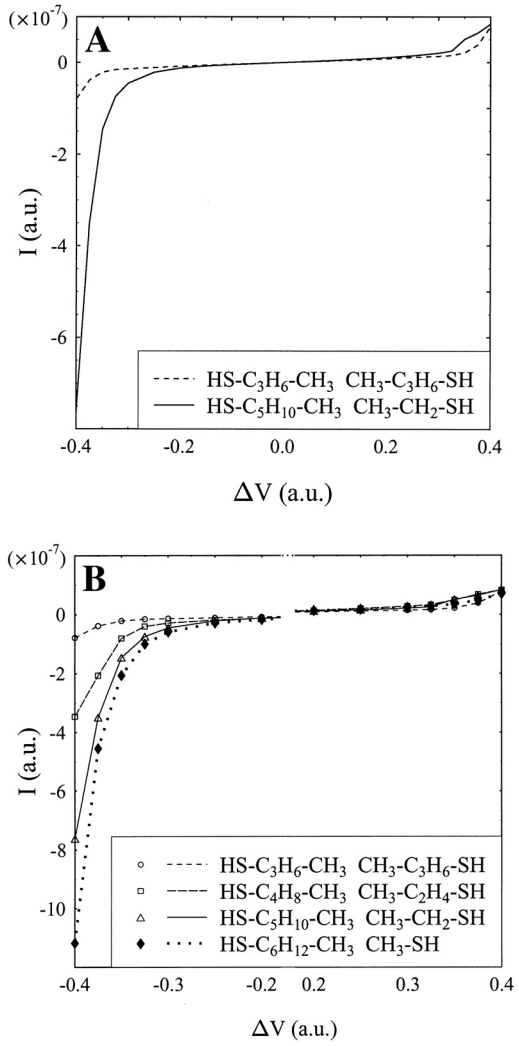

FIGURE 3. A. Current versus applied voltage obtained from a NEGF-HF calculation for the symmetric ($n = m = 3$, *dashed line*) and asymmetric ($n = 5$, $m = 1$, *solid line*) junctions. Here and in the following figures *circles* and *triangles* denote the points where actual calculations were made. **B.** Similar results computed for eight-carbon junctions of variable asymmetry.

in our calculation is neglect of the electronic response of the electrodes (image interactions) to the tunneling electron.

FIGURE 4 shows the energies of MOs as functions of the applied voltage for the symmetric and asymmetric junctions. The straight lines are chemical potentials,

$\mu_L = E_F - eV_L$ and $\mu_R = E_F - eV_R$, of the leads. The gray area between these lines represents the energy region relevant for current calculation at low temperatures due to the $f_L(E) - f_R(E)$ factor in Eq. **(24)**. We note that, although for the symmetric junction the MOs behave in a symmetric way with respect to the change of voltage polarity, the asymmetric junction shows a slight asymmetry: the HOMO on the left ($\Delta V < 0$) side of FIGURE 4B enters the relevant region slightly earlier (i.e., at smaller voltage) than on the right ($\Delta V > 0$) side, thus leading to an earlier current increase for the negatively biased junction. It is encouraging to find that conduction is dominated by the HOMO, which is described better than LUMO in the HF approximation.

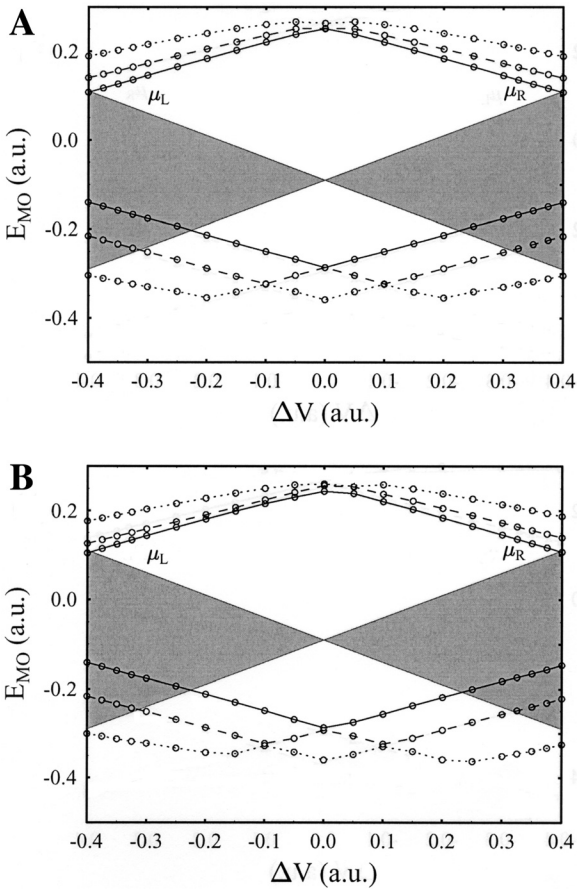

FIGURE 4. Molecular orbitals of the entire bimolecular bridge versus applied voltage for **(A)** the symmetric and **(B)** the asymmetric junctions. Shown are the HOMO (*solid line*) and two MOs immediately below it (*dashed* and *dotted lines*) as well as the LUMO (*solid line*) and two MOs immediately above it (*dashed* and *dotted lines*). The *circles* denote the voltage points for which calculations were made (the lines interpolate between these points). Also shown are electrochemical potentials (*straight lines*) of the electrodes.

A more important insight is obtained from comparing FIGURE 4 and FIGURE 5. The latter shows, as functions of applied voltage, the MOs of the disconnected left and right segments of the bimolecular bridge. The symmetric junction is again characterized by a symmetric behavior (FIG. 5A), whereas the asymmetric junction again shows a slight asymmetry in the corresponding energies (FIG. 5B). More important, however, is the asymmetry in the nature of the wave functions. Comparing FIGURES 4B and 5B one sees that the HOMO of the total bridge (the orbital responsible for the current buildup) is dominated on the right side ($\Delta V > 0$) by the HOMO of the right (short) molecular segment, but in the left side ($\Delta V < 0$) the main contribution

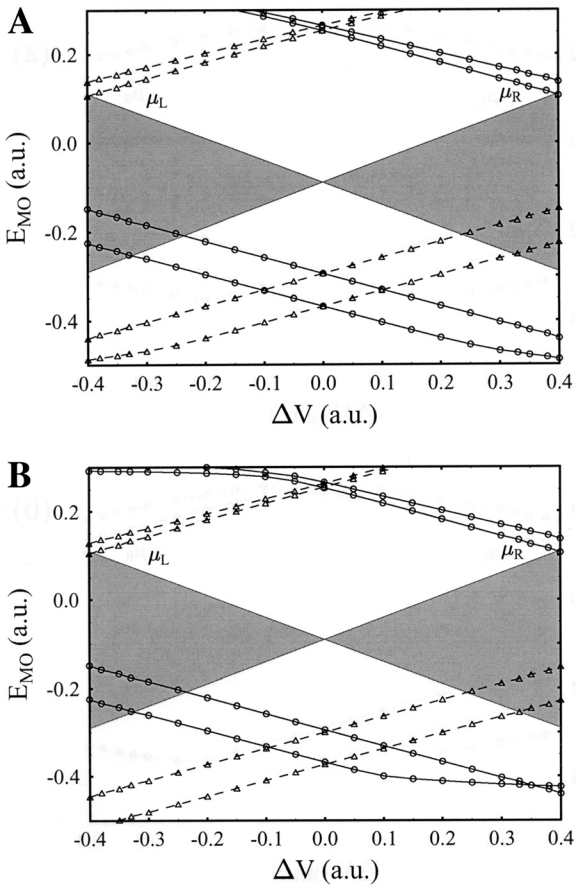

FIGURE 5. Molecular orbitals of the individual molecular segments of the bridge versus applied voltage for **(A)** the symmetric ($n = m = 3$) and **(B)** the asymmetric ($n = 5$, $m = 1$) junctions. Shown is the HOMO with the level immediately below it and the LUMO with the level immediately above it for the left (*solid lines* and *circles*) and right (*dashed lines* and *triangles*) molecular segments. Also shown are the chemical potentials (*straight lines*). The *circles* and *triangles* denote points where actual calculations were made.

comes from the HOMO of the left (long) part of the molecule. This observation is consistent with the calculated overlap between the total bridge HOMO and various atomic orbitals of the molecule. The observation implies that for a positively biased ($\Delta V > 0$) junction the bridge HOMO is localized on the short (right) molecular segment, thus the other (long) molecular segment represents an effective barrier for electron tunneling, which results in a small current through the junction. For the negatively biased ($\Delta V < 0$) junction, on the other hand, the total bridge HOMO is localized on the long (left) molecular segment, thus an effective barrier for electron

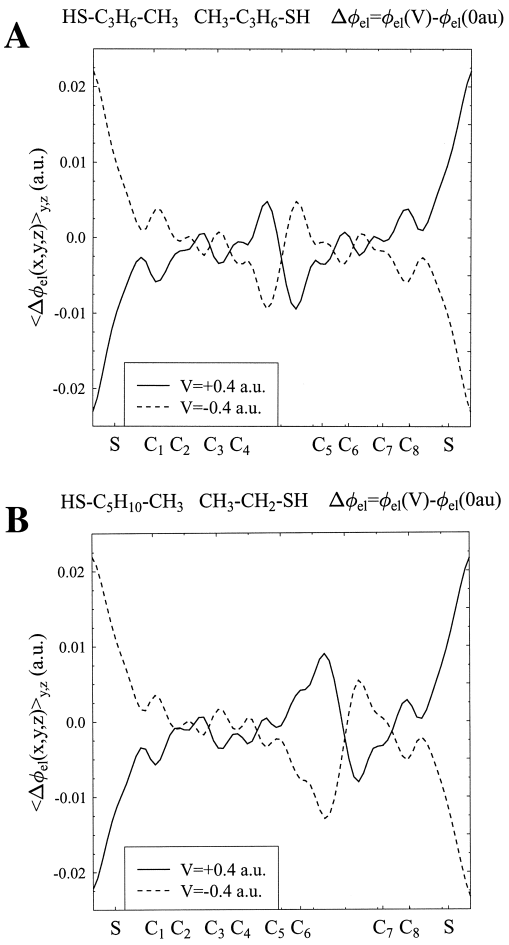

FIGURE 6. Difference between total potential profile across the molecular junction at voltage drop ΔV and at equilibrium ($\Delta V = 0$). Shown are two curves at opposite voltage biases: $\Delta V = +0.4$ a.u. (*solid curve*) and $\Delta V = -0.4$ a.u. (*dashed curve*) for **(A)** the symmetric ($n = m = 3$) and **(B)** the asymmetric ($n = 5$, $m = 1$) junctions. The value of the potential was obtained by averaging in the C–C–C plane of the molecule.

tunneling is represented by the short part of the molecule, which leads to a larger current for this voltage polarity than in the opposite case. A similar mechanism for current–voltage asymmetry was proposed in a different context in Reference 22.

Finally, FIGURE 6 shows the total potential profile across the molecular junction as obtained from the NEGF-HF calculation. Shown is the difference between the electrostatic potential at voltage drop ΔV and at equilibrium ($\Delta V = 0$). This is done to exclude the nuclear contribution ϕ_{nuc} (see Eq. **(26)**) which is much larger in magnitude and whose inclusion would obscure the shape of potential drop. The potential is plotted as a function of distance along the molecular axis (a line connecting the midpoints of all the C–C bonds), and the value shown at each point is an average over a linear range (± 3 Å) normal to this axis in the C–C–C plane, in which the potential is appreciable. Results are presented for the symmetric and asymmetric junctions. Each graph shows two curves corresponding to different voltage drop polarities: $\Delta V = +0.4$ a.u. (solid line) and $\Delta V = -0.4$ a.u. (dashed line). Considerable voltage drop takes place at the molecule–electrode interfaces as well as at the gap between the two molecular segments of the junction.

It is important to note that the existence of this weak link, placed asymmetrically between the metal leads is essential for the observed current–voltage asymmetry. That this should be so is obvious because this is the only source of asymmetry in the system. Perhaps less obvious is the weak link property of this asymmetric element that implies, as mentioned above, a substantial potential drop across it. Indeed, an extended Huckel calculation on the same system, in which the potential profile is not computed self-consistently but is imposed as an additional model input, shows no rectification unless a potential drop across the intermolecular gap is imposed.[25] This gap is seen to act as an effective molecular capacitor, with opposite charges accumulating on the corresponding molecular edges. This suggests the possibility of using molecular junctions with weak links as capacitive elements in nanoelectronics.

CONCLUSIONS

We have presented a procedure, based on the NEGF-HF formalism, for calculating the electronic transport properties of molecular junctions, and have applied it to interpret the observed symmetry properties of the current–voltage characteristic of alkanethiol bilayer adsorbed on metal electrodes. An effective procedure for calculating transport properties based on the NEGF method at the HF level was described. The computed *I–V* asymmetry is in accord with experimental observations.

Both asymmetry in the molecular structure and the occurrence of a potential drop at the intermolecular gap were found to be necessary elements for observing asymmetric response. The structural weak link—the van-der-Waals gap between the two alkyl chains—provides both the needed asymmetry and the essential potential drop. This gap essentially constitutes a molecular-scale capacitor and the observed phenomenon suggests that such structures may be used as capacitive elements in molecular electronic devices. Obviously, the full electronic implications of such a structure in current carrying junctions can be studied only within a non-equilibrium theory that includes electron–electron interactions. The NEGF-HF method is an example (at the simple HF level) of such consideration.

Our calculation has pointed out a reasonable mechanism for the observed rectifying action, which seems to be generic to asymmetric structures involving weak links: at opposite biases, the charge carriers are localized on molecular segments of different length, leading to different widths of the effective barrier to tunneling experienced in the two cases.

The computational method described and used above is an NEGF based method, similar in spirit to several other recent calculations (see e.g., Refs. 10 and 32–34). However, it is simpler to implement due to the efficient integration procedure described in the APPENDIX. Its possible generalization; for example, in the spirit of divide-and-conquer methods used for studying electron transport in large (biological) molecules[35,36] would make it possible to apply these concepts to other electron transfer processes. Such generalizations would also require the consideration of electron–phonon interactions. Even though this is formally straightforward, it will take much effort to make such a calculation numerically efficient and further studies in these directions are desirable.

ACKNOWLEDGMENTS

This work was supported by the U.S.–Israel Binational Science Foundation, the Israel Academy of Science and the Wolkswagen Foundation. We are indebted to Professor M. Majda whose communication of the experimental results by Sek and Majda initiated our theoretical efforts on this issue, and to Professor L. Halperin for helpful discussions on mathematical techniques. M.G. gratefully acknowledges the hospitality and support of Professor D. Beratan at Duke University.

APPENDIX: LARGE SYSTEMS AT HF LEVEL

The main complexity in the NEGF calculations for large molecular systems stems from the need to evaluate and store Green's function (GF) matrices for many energies, required for the evaluation of integrals, such as **(21)**. Depending on the structure of the integrand (e.g., number and sharpness of resonance), we may encounter the need to do such calculations on a fine energy grid. Note that simple contour integration in the complex plane, which is useful in the zero temperature case, is difficult at finite temperature due to the poles of the Fermi–Dirac distribution function that enter the integrand. At each energy point we need to evaluate the GF (inversion of the big matrix) and sometimes store it, implying a big demand on CPU time and memory. Here we present an approach that overcomes both limitations and can be used for NEGF calculations of big systems. The method described below is valid in cases where the self-energy due to the electrodes can be taken energy-independent (the so called wide-band limit of the external reservoir, see e.g., Ref. 6) and the self-energies arising from other (i.e., interparticle) interactions are only of the irregular type—that is, time-local. The latter implies that the corresponding lesser and greater self-energies vanish whereas the retarded (advanced) self-energies are again energy independent (for steady-state situations; see Refs. 37 and 38), as is the case for the

electron–electron interaction in the HF of approximation and for the interaction with a time-constant external potential.

Hamiltonian and Green Functions

The reduced Hamiltonian for the molecular bridge, obtained by projecting out the electrode subspaces, may be written, for example, in the basis of Löwdin orbitals, in the form

$$\mathbf{H} = \mathbf{H}_c + \mathbf{\Sigma}^r, \tag{A1}$$

where $\mathbf{H}_c$ is the core Hamiltonian (the first term of Eq. **(3)**) and $\mathbf{\Sigma}^r$ is the retarded self-energy, consisting of all contributions according to **(14)**. The Hamiltonian **(A1)** can be diagonalized using

$$\mathbf{HU} = \mathbf{UH}_d \Leftrightarrow \mathbf{H} = \mathbf{UH}_d\mathbf{U}^{-1}, \tag{A2}$$

where $\mathbf{U}$ is a matrix formed from columns of the right eigenvectors of the complex matrix $\mathbf{H}$, and $\mathbf{H}_d$ is a diagonal matrix of the complex eigenvalues $\{E_n\}$ $(n = 1,\ldots,N)$ of $\mathbf{H}$. The retarded GF is

$$\mathbf{G}^r(\mathbf{E}) = [\mathbf{E} - \mathbf{H}]^{-1} = \mathbf{U}[\mathbf{E} - \mathbf{H}_d]^{-1}\mathbf{U}^{-1} \tag{A3}$$

or

$$G^r_{ij}(E) = \sum_l U_{il}\frac{1}{E - E_l}(U^{-1})_{lj}. \tag{A4}$$

The poles E_l satisfy $E_l = \varepsilon_l - i\gamma_l$, where $\gamma_l > 0$.

The matrix elements of the advanced GF, $G^a(E) = [G^r(E)]^+$, are given by

$$G^a_{ij}(E) = \sum_l (\mathbf{U}^{-1})^*_{li}\frac{1}{E - E^*_l}U^*_{jl}. \tag{A5}$$

The corresponding lesser and greater GFs can be obtained from the Keldysh equation, **(23)**. The result is

$$\begin{aligned} G^<_{ij}(E) &= i\sum_{p,r} U_{ip}(W^L_{pr}f_L(E) + W^R_{pr}f_R(E))U^*_{jr} \times \frac{1}{E - \varepsilon_p + i\gamma_p}\frac{1}{E - \varepsilon_r - i\gamma_r} \\ G^>_{ij}(E) &= -i\sum_{p,r} U_{ip}(W^L_{pr}[1 - f_L(E)] + W^R_{pr}[1 - f_R(E)])U^*_{jr} \times \frac{1}{E - \varepsilon_p + i\gamma_p}\frac{1}{E - \varepsilon_r - i\gamma_r} \end{aligned} \tag{A6}$$

where

$$W^K_{pr} = \sum_{s,t}(U^{-1})_{ps}\Gamma^K_{st}(U^{-1})^*_{rt}, \quad K = L, R, \tag{A7}$$

and the matrix Γ is defined by Eq. **(25)**.

The Density Matrix

The main numerical problem we face is the need to do the energy integrals that appear in many of expressions of interest, Eq. **(21)** for the density matrix, for example. In the general case such integral have to be done numerically and this constitutes the main numerical obstacle in the application of the NEGF to practical problems. Under our assumptions the retarded self-energy is energy independent, whereas the energy dependence of the lesser and greater projections is known (compare with Eqs. **(18)**). Using **(A6)** in **(21)** leads to

$$P_{ij} = \sum_{K=L,R} \sum_{p,r} \{U_{ip} W^K_{pr} I^K_{pr} U^*_{jr}\}, \tag{A8}$$

where

$$I^K_{pr} = \int_{-\infty}^{\infty} \frac{dE}{2\pi} \frac{1}{E - \varepsilon_p + i\gamma_p} \frac{1}{E - \varepsilon_r - i\gamma_r} f_K(E). \tag{A9}$$

This integral can be evaluated exactly, as described below.

Evaluation of the Integral (A9)

Consider the integral

$$\begin{aligned} I &= \int_{-\infty}^{\infty} \frac{dE}{2\pi} \frac{1}{E - \varepsilon_1 + i\gamma_1} \frac{1}{E - \varepsilon_2 - i\gamma_2} \frac{1}{\exp[\beta(E-\mu)] + 1} \\ &= \frac{\beta}{2\pi} \int_{-\infty}^{\infty} dx \frac{1}{x - \beta(\varepsilon_1 - \mu - i\gamma_1)} \frac{1}{x - \beta(\varepsilon_2 - \mu + i\gamma_2)} \frac{1}{e^x + 1}. \end{aligned} \tag{A10}$$

The last equality is obtained by using $x = \beta(E - \mu)$. The integral can be evaluated by contour integration. The integrand has simple poles at (see FIGURE 7).

$$\begin{aligned} x &= x_1 \equiv \beta(\varepsilon_1 - \mu - i\gamma_1) \\ x &= x_2 \equiv \beta(\varepsilon_2 - \mu + i\gamma_2) \\ x &= y_n \equiv i(\pi + 2\pi n) \quad n = 0, \pm 1, \ldots . \end{aligned} \tag{A11}$$

One can close the contour of integration either along the C_1 or the C_2 curves (FIG. 7). Accordingly we obtain

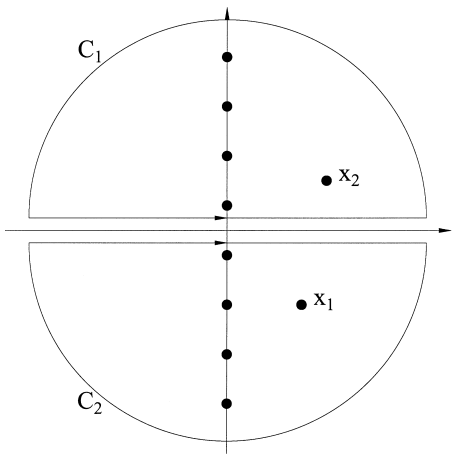

FIGURE 7. Contours and poles in the complex plane. See text for details.

$$I = \begin{cases} i\beta\left[\dfrac{1}{x_2 - x_1}\dfrac{1}{e^{x_2}+1} - \displaystyle\sum_{n=0}^{\infty}\dfrac{1}{(y_n - x_1)(y_n - x_2)}\right]; & C_1 \\ i\beta\left[\dfrac{1}{x_2 - x_1}\dfrac{1}{e^{x_1}+1} - \displaystyle\sum_{n=0}^{\infty}\dfrac{1}{(y_n + x_1)(y_n + x_2)}\right]; & C_2 \end{cases} \tag{A12}$$

These sums can be written in terms of known special functions. Using[39]

$$\sum_{n=0}^{\infty}\frac{1}{(n+a)(n+b)} = \frac{1}{b-a}[\psi(b) - \psi(a)], \tag{A13}$$

where

$$\begin{aligned} \psi(z) &= \frac{\Gamma'(z)}{\Gamma(z)} \quad \text{psi (digamma) function} \\ \Gamma(z) &= \int_0^{\infty} dt t^{z-1}e^{-t} \quad \text{gamma function,} \end{aligned} \tag{A14}$$

we obtain

$$I = \begin{cases} \dfrac{i\beta}{x_2 - x_1}\left[\dfrac{1}{e^{x_2}+1} - \dfrac{i}{2\pi}\left\{\psi\left(\dfrac{1}{2} + i\dfrac{x_2}{2\pi}\right) - \psi\left(\dfrac{1}{2} + i\dfrac{x_1}{2\pi}\right)\right\}\right]; & C_1 \\ \dfrac{i\beta}{x_2 - x_1}\left[\dfrac{1}{e^{x_1}+1} - \dfrac{i}{2\pi}\left\{\psi\left(\dfrac{1}{2} - i\dfrac{x_2}{2\pi}\right) - \psi\left(\dfrac{1}{2} - i\dfrac{x_1}{2\pi}\right)\right\}\right]; & C_2 \end{cases} \tag{A15}$$

One can show that the two results are equal by using[40]

$$\psi(1-z) = \psi(z) + \pi\cot(\pi z). \tag{A16}$$

Numerical evaluation of the psi (digamma) function is, however, difficult. Instead, in our numerical calculation we use the following simple scheme for evaluation of the infinite sums in **(A12)**. For each sum let $S_N = \sum_{n=0}^{N} \ldots$, and choose N large enough so that the rest of the sum may be evaluated as an integral. This leads to

$$\sum_{n=0}^{\infty}\frac{1}{(y_n \mp x_1)(y_n \mp x_2)} = S_N - \frac{1}{(2\pi)^2}\left\{\frac{1}{N+1} - \frac{1 \pm i\dfrac{x_1 + x_2}{2\pi}}{2(N+1)^2}\right\}. \tag{A17}$$

The evaluation of I is then reduced to summation to obtain S_N an easy numerical task.

REFERENCES

1. DATTA, S. 1995. Electric Transport in Mesoscopic Systems. Cambridge University Press, Cambridge.
2. NITZAN, A. 2001. Electron transmission through molecules and molecular interfaces. Ann. Rev. Phys. Chem. **52:** 681–750.

3. KELDYSH, L.V. 1965. Diagram technique for nonequilibrium processes. Sov. Phys. JETP **20:** 1018–1026.
4. KADANOFF, L.P. & G. BAYM. 1962. Quantum Statistical Mechanics. Green's Function Methods in Equilibrium and Nonequilibrium Problems. W.A. Benjamin, New York.
5. DATTA, S., W.D. TIAN, S.H. HONG, *et al.* 1997. Current–voltage characteristics of self-assembled monolayers by scanning tunneling microscopy. Phys. Rev. Lett. **79:** 2530–2533.
6. TIAN, W., S. DATTA, S. HONG, *et al.* 1998. Conductance spectra of molecular wires. J. Chem. Phys. **109:** 2874–2882.
7. MUJICA, V., A.E. ROITBERG & M. RATNER. 2000. Molecular wire conductance: electrostatic potential spatial profile. J. Chem. Phys. **112:** 6834–6839.
8. HIROSE, K. & M. TSUKADA. 1995. First principles calculation of the electronic structure for a bielectrode junction system under strong field and current. Phys. Rev. B **51:** 5278–5290.
9. LANG, N.D. & P.H. AVOURIS. 2000. Carbon-atom wires: charge-transfer doping, voltage drop, and the effect of distortions. Phys. Rev. Lett. **84:** 358–361.
10. DAMLE, P.S., A. W. GOSH & S. DATTA. 2001. Unified description of molecular conduction: From molecules to metallic wires. Phys. Rev. B **64:** 201403.
11. NITZAN, A., M. GALPERIN, G.-L. INGOLD & H. GRABERT. 2002. On the electrostatic potential profile in biased molecular wires. J. Chem. Phys. **117:** 10837–10841.
12. PLEUTIN, S., H. GRABERT, G.-L. INGOLD & A. NITZAN. 2003. The electrostatic potential along a biased molecular wire. J. Chem. Phys. **118:** 3656–3763.
13. METZGER, R.M. 1999. Electrical rectification by a molecule: the advent of unimolecular electronic devices. Acc. Chem. Res. **32:** 950–957.
14. CHABINYC, M.L., X.X. CHEN, R.E. HOLMLIN, *et al.* 2002. Molecular rectification in a metal–insulator–metal junction based on self-assembled monolayers. J. Am. Chem. Soc. **124:** 11730–11736.
15. OKAZAKI, N., J.R. SAMBLES & G.J. ASHWELL. 2002. Molecular rectification at 8 K in an Au/C(16)H(33)Q-3CNQ LB film/Au structure. Appl. Phys. Lett. **81:** 2300–2302.
16. FISCHER, C.M., M. BURGHARD & S. ROTH. 1995. Molecular rectification in organic quantum-wells. Synthetic Metals **71:** 1975–1976.
17. FISCHER, C.M., M. BURGHARD, S. ROTH & K. VONKLITZING. 1994. Organic quantum-wells—molecular rectification and single-electron tunneling. Europhys. Lett. **28:** 129–134.
18. MARTIN, A.S. & J.R. SAMBLES. 1993. Further evidence for molecular rectification in M/LB/M junctions. Mol. Cryst. Liq. Cryst. A **234:** 679–684.
19. SAMBLES, J.R. & A.S. MARTIN. 1993. Molecular rectification. Phys. Scripta **T49B:** 718–720.
20. ROTH, S., S. BLUMENTRITT, *et al.* 1998. Density of states and tunneling spectroscopy on molecular nanostructures. Thin Solid Films **331:** 45–50.
21. AVIRAM, A. & M.A. RATNER. 1974. Molecular rectifiers. Chem. Phys. Lett. **29:** 277–283.
22. WALDECK, D.H. & D.N. BERATAN. 1993. Molecular electronics: observation of molecular rectification. Science **261:** 576–577.
23. MARCUS, R.A. 1996. Symmetry or asymmetry of k_{ET} and I_{STM} versus potential curves. J. Chem. Soc. Faraday Trans. **92:** 3905–3908.
24. MUJICA, V., M. RATNER & A. NITZAN. 2002. Molecular rectification: why is it so rare? Chem. Phys. **281:** 147–150.
25. GALPERIN, M., A. NITZAN, S. SEK & M. MAJDA. 2003. Asymmetric electron transmission across asymmetric alkanethiol bilayer junctions. J. Electroanal. Chem. **550–551:** 337–350.
26. LOWDIN, P.-O. 1950. On the non-orthogonality problem connected with the use of atomic wave functions in the theory of molecules and crystals. J. Chem. Phys. **18:** 365–375.
27. HAUG, H. & A.-P. JAUHO. 1996. Quantum Kinetics in Transport and Optics of Semiconductors. Springer, Berlin.

28. SAUNDERS, V.R. 1982. Molecular integrals for Gaussian type functions. *In* Methods in Computational Molecular Physics, Vol. 113. G.H.F. Diercksen & S. Wilson, Eds.: 1–36. D. Reidel Publishing Company, Dordrecht.
29. SHAVITT, I. 1963. The Gaussian function in calculations of statistical mechanics and quantum mechanics. *In* Methods in Computational Physics. Advances in Research and Applications, Vol. 2. B. Adler, S. Fernbach & M. Rotenberg, Eds.: 1–45. Academic Press, New York.
30. FRISCH, M.J., G.W. TRUCKS, *et al.* 2001. A./X revision. Gaussian Inc., Pittsburgh.
31. YALIRAKI, S.N., A.E. ROITBERG, C. GONZALES, *et al.* 1999. The injecting energy at molecule/metal interfaces: implications for conductance of molecular junctions from an *ab initio* molecular description. J. Chem. Phys. **111:** 6997–7002.
32. TAYLOR, J., H. GUO & J. WANG. 2001. *Ab initio* modeling of open systems: charge transfer, electron conduction, and molecular switching of a C_{60} device. Phys. Rev. B **63:** 121104.
33. TAYLOR, J., H. GUO & J. WANG. 2001. *Ab initio* modeling of quantum transport properties of molecular electronic devices. Phys. Rev. B **63:** 245407.
34. BRANDBYGE, M., J.-L. MOZOS, *et al.* 2002. Density-functional method for nonequilibrium electron transport. Phys. Rev. B **65:** 165401.
35. YANG, W. 1991. Direct calculation of electron density in density-functional theory. Phys. Rev. Lett. **66:** 1438–1441.
36. YANG, W. & T.-S. LEE. 1995. A density-matrix divide-and-conquer approach for electronic structure calculations of large molecules. J. Chem. Phys. **103:** 5674–5678.
37. DANIELEWICZ, P. 1984. Quantum theory of nonequilibrium processes, I. Ann. Phys. **152:** 239–304.
38. WAGNER, M. 1991. Expansions of nonequilibrium Green's functions. Phys. Rev. B **44:** 6104–6117.
39. PRUDNIKOV, A.P., Y.A. BRYCHKOV & O.I. MARICHEV. 1981. Integrals and Series. Nauka, Moscow.
40. ABRAMOWITZ, M. & I.A. STEGUN, Eds. 1964. Handbook of Mathematical Functions with Formulas, Graphs, and Mathematical Tables. National Bureau of Standards.